- 1 Modeling the mechanisms of coastal vegetation dynamics and ecosystem responses to changing
- 2 water levels
- 3 Junyan Ding,¹ Nate McDowell^{2,3}, Vanessa Bailey², Nate Conroy,⁴ Donnie J. Day,⁵ Yilin Fang,⁶
- 4 Kenneth M. Kemner, Matthew L. Kirwan, Charlie D. Koven, Matthew Kovach, Patrick
- 5 Megonigal,¹⁰ Kendalynn A. Morris,¹¹ Teri O'Meara,¹² Stephanie C. Pennington,¹¹ Roberta B.
- 6 Peixoto, ⁵ Peter Thornton, ¹² Mike Weintraub, ⁵ Peter Regier, ¹³ Leticia Sandoval, ⁵ Fausto
- 7 Machado-Silva,⁵ Alice Stearns,¹⁰ Nick Ward,¹³ Stephanie J. Wilson¹⁰

8

- 9 1. Department of Biology, Occidental College, Los Angeles, CA, USA, 90041
- Biological Science Division, Pacific Northwest National Laboratory, Richland, WA, USA,
 99352
- School of Biological Sciences, Washington State University, PO Box 644236, Pullman, WA,
 USA, 99164-4236
- 4. Earth and Environmental Sciences Division, Los Alamos National Laboratory, New Mexico,
 USA, 87545
- 16 5. The University of Toledo, Toledo, OH, USA, 43606
- Earth Systems Science Division, Pacific Northwest National Laboratory, Richland, WA,
 USA, 99352
- Molecular Environmental Sciences Group, Argonne National Laboratory, Lemont, IL, USA
 60439
- 8. Virginia Institute of Marine Science, College of William and Mary, Gloucester Point, VA,
 USA, 23062
- Climate and Ecosystem Sciences Division, Lawrence Berkeley National Laboratory,
 Berkeley, USA
- 25 10. Smithsonian Environmental Research Center, Edgewater, MD, USA, 21037
- 26 11. Joint Global Change Research Institute, Pacific Northwest National Laboratory, College
 27 Park, MD, USA, 20740
- 28 12. Environmental Sciences Division, Oak Ridge National Laboratory, Oak Ridge, TN, USA, 37830
- 13. Marine and Coastal Research Laboratory, Pacific Northwest National Laboratory, Sequim,
 WA, USA, 98382

32

33 Corresponding author: Junyan Ding, jding@oxy.edu

Abstract

Coastal forests are increasingly experiencing mortality due to inundation by fresh- and seawater, leading to their replacement by marshes. These shifts alter vegetation composition, biogeochemical cycling, carbon storage, and hydrology. Using a hydraulically enabled ecosystem demography model (FATES-Hydro), we conducted numerical experiments to investigate the mechanisms behind inundation-driven forest loss and the ecosystem-scale consequences of forest-to-marsh transitions. We compared mortality processes and their effects across broadleaf and conifer trees at two coastal sites—Lake Erie (freshwater) and Chesapeake Bay (saline).

Our simulations show that hydraulic failure, driven by root loss under prolonged flooding, is the primary mortality mechanism across both tree types and sites. Forest replacement by marsh reduced ecosystem-scale leaf area index (LAI), gross primary production (GPP), transpiration, and deep soil water uptake in conifer forests, while broadleaf forests experienced smaller changes due to lower initial LAI and greater marsh compensation. Marsh invasion occurred following canopy thinning driven by tree mortality. These findings suggest that, under similar root loss, hydraulic failure dominates coastal tree mortality regardless of species or water type, with denser forests experiencing stronger ecosystem impacts. Our study identifies key mortality mechanisms and offers testable hypotheses for future empirical studies on coastal vegetation change.

Page 2 of 33

1 Introduction:

2021; Yadav et al., 2011).

Shoreline vegetation provides important ecosystem functions (Barbier et al., 2011; Mitsch et al., 2015). Coastal forests can be more productive than adjacent upland systems (Tagestad et al., 2021), have larger carbon stocks than the marshes replacing them (Smith et al. 2021), mitigate storm-driven erosion (Arkema et al., 2013; Spalding et al., 2014), and provide habitat for a wide variety of animals (Duarte et al., 2013; Barbier, 2013; Mitsch et al., 2015). Coastal ecosystems are experiencing rapid increases in tree mortality due to changing water levels in both fresh- and seawater systems (McDowell et al. 2022). Globally, sea-level rise and flooding threaten coastal forests, with potential habitat losses ranging from less than 10% with a 1-meter rise to as much as 55% under a 3-meter rise scenario (Ury et al., 2021). Increasingly variable freshwater levels in lakes and accelerating sea level rise (SLR) are anticipated with climate change (Varekamp et al., 1992; Mimura, 2013; Theuerkauf et al., 2019; Kayastha et al., 2022; Saber et al., 2023). Varying water levels induce large changes in species composition, including shifts from forest to marsh, driven in part by tree mortality (Keddy and Reznicek, 1986; Hudon, 1997; Frieswyk and Zedler, 2007; Wilcox, 2004; Wilcox and Nichols, 2008).

Soil hypoxia and salinity are key drivers of tree mortality under increasing inundation. Prolonged increases in hypoxia and soil salinity reduce root hydraulic conductance and promote root loss (Colmer and Flowers, 2008; Pezeshki, 2001). Elevated soil salinity also reduces soil water potential (Boursiac et al., 2005), thereby reducing the soil-to-root water potential gradient that drives water movement into roots. Together, these belowground impacts of rising hypoxia and salinity reduce whole-plant hydraulic conductivity (López-Berenguer et al., 2006; Nedjimi, 2014), subsequently increasing the likelihood of xylem embolism and mortality from hydraulic failure (McDowell et al., 2022). These reductions in whole-plant conductivity can promote carbon starvation through declining stomatal conductance (Orsini et al., 2012; Sperry et al., 2016) and leaf loss (Munns and Termaat, 1986; Wang et al., 2019; Zhang et al., 2021b). Increased salt concentrations inhibit potassium accumulation in guard cells, also promoting stomatal closure (Clough and Simm, 1989; Perri et al., 2019). These photosynthetic constraints can be exacerbated by foliar ion toxicity that impairs photosynthetic biochemistry (Ball and Farquhar, 1984; Delatorre-Herrera et al., 2021; Munns, 2005; Suárez and Medina, 2006; Li et al.,

Physiological impacts from hypoxia and salinity can also vary with the frequency and duration of inundation and with interspecific variation in physiological traits. Freshwater systems experience variable inundation across seasons and years (Fig. 1) and may have opportunity to recover from inundation, whereas SLR induces a chronic rise in inundation that can reduce recovery (Taherkhani et al., 2020; Thiéblemont et al. 2023). Interspecific trait differences such as in xylem vulnerability to cavitation can also influence the degree of mortality (Niknam and McComb, 2000; Lukac et al., 2000; Sairam et al., 2008; Acosta-Motos et al., 2017; Zhao et al., 2020; McDowell et al. 2022). Mortality mechanism tests have not addressed inundation dynamics and interspecific variation.

Coastal tree mortality has large impacts on ecosystem function (Kirwan and Gedan, 2011). Tree mortality reduces forest biomass and leaf area (Chen and Kirwan, 2022), which in turn provides a light environment favorable for the expansion of marsh vegetation (Shaw et al., 2022; Sward et al., 2023). This results in transpiration and carbon uptake and storage shifting from trees to marsh plants as forests retreat, with net reductions in fluxes and storage depending on the degree of compensation by the invading marsh (Smith et al., 2021; Davidson et al., 2018; Zhou et al., 2023). However, the effects of tree death and marsh invasion on ecosystem-scale fluxes and their underlying mechanisms are poorly known (Kirwan et al., 2024).

In a recent study, Ding et al. (2023b) incorporated the effects of salinity and hypoxia on root loss, hydraulic function, and photosynthesis into the process-based ecosystem demographic model FATES-Hydro to simulate physiological responses of conifer trees to seawater exposure. They applied the model to three coastal conifer forests in the U.S., finding that both hydraulic failure and carbon starvation contribute to tree mortality, with the dominant mechanism depending on the rate and duration of salinization. Rapid exposure favored carbon starvation, while chronic inundation led primarily to hydraulic failure.

Building upon Ding et al. (2023b), which focuses on physiological responses of conifer trees to seawater exposure, here we extend the investigation to broadleaf deciduous trees, allowing evaluation of how functional traits such as photosynthetic capacity, morphology, and phenology influence mortality outcomes under similar belowground stress conditions. Because the two tree functional groupstypes have very different physiology, morphology and phenology, we specifically examine to which extent the difference in these traits can affect the response of trees

116 to hypoxia and salinity if root loss are the same. We also incorporate a freshwater coastal system 117 (Lake Erie) alongside a saline coastal site to compare how hydrologic context shapes vegetation 118 transitions. We further assess ecosystem-scale consequences of tree mortality, including its 119 impact on vegetation composition, and ecosystem fluxes. We conducted numerical experiments 120 using Ding et al.(2023b) FATES-Hydro with a reciprocal design where the two tree functional 121 groupstypes were simulated for both the freshwater and saline coasts to partition the role of 122 species from their environment. We expect the broadleaf deciduous trees will be more 123 susceptible to carbon starvation particular at saline coastal than conifers. 124 2. Methods 125 2.1 Study areas 126 The first site is located on the south shore of Lake Erie (the LE site) in Ohio, USA (41.48°N, 127 83.06°W) (Fig. S1). The area has warm and humid summers and cold winters. The LE site is 128 dominated by the broadleaf species shellbark hickory (Carya laciniosa) and swamp white oak 129 (Quercus bicolor). Lake Erie is part of the Great Lakes of North America, a series of 130 interconnected large freshwater lakes. The water level of Lake Erie is subject to daily, seasonal, 131 interannual, and decadal variation resulting from the complex interactions between climate, 132 bathymetry, and the water levels of the upper lakes (Burlakova et al., 2014). Increases in the 133 water levels in Lake Erie have resulted in extensive coastal tree mortality (Sippo et al., 2018; 134 Theuerkauf and Braun, 2021). 135 The second site is located on the Chesapeake Bay (CB) in Maryland, USA (38.5°N, 76.3°W; 136 Smith and Kirwan 2021) (Fig. S1). The CB site is dominated by coniferous loblolly pine (*Pinus* 137 taeda) forests, and the climate is characterized by warm, humid summers and cool winters. The 138 CB region is a hotspot for sea-level driven coastal forest retreat, driven in part by the extensive 139 low lying coastal plain topography (Schieder et al., 2018; Chen and Kirwan, 2022). In the 20th 140 21st century, relative SLR rates in the CB region (~3 to 6 mm per year) are approximately two to 141 three times faster than the global average (Sallenger et al., 2012; Ezer and Corlett, 2012). 142 In 2022, two forested study plots were established within the dying shoreline forests and in 143 the neighboring unflooded uplands at each site. Stand level measurements include tree density, 144 diameter at breast height (DBH) and water table depth. Tree-specific measurements were taken

from eight live trees in each plot, which included growth, non-structural carbohydrates,

146	continues hourly sap flow, leaf gas exchange, leaf photosynthetic capacity, and hourly leaf water
147	potential (LWP) including predawn and mid-day LWP of a given day during the growing season.
148	These eight live trees were bored to obtain tree cores for measurements of ring width growth
149	along with eight dead trees located at the shoreline. We follow exactly the same measurements
150	and sample processing as described in Zhang et al. (2021), Wang et al. (2020). Here, we
151	benchmarked the FATES-Hydro model against empirical data collected at each site.
152	
153	2.2 Numerical experiments with the FATES-Hydro model
154	We conducted numerical experiments at both the LE and CB sites using a newly developed
155	version of the ecosystem demography model, FATES-Hydro (Ding et al. 2023b), which
156	represents the physiological impacts of hypoxia and salinity on plants and consequent changes in
157	root conductance and mortality. <u>All simulations were run with FATES-Hydro within the E3SM</u>
158	Land Model (ELM). Here we describe this version of FATES-Hydro, its parameterization and
159	benchmarking for this study, and the design of the numerical experiments.
160	2.2.1 Description of FATES-Hydro
161	The Functionally Assembled Terrestrial Ecosystem Simulator (FATES) is a physiology-based
162	vegetation demographic model that simulates cohort-scale dynamics for different plant
163	functional types (PFTs) (Fisher et al., 2018; Koven et al., 2020). FATES-Hydro is a version that
164	integrates the plant hydraulics and their coupling with photosynthesis (Ding et al., 2023a). In
165	FATES-Hydro plant transpiration is the product of whole-plant leaf area and the transpiration
166	rate per unit leaf area (J), which itself is the product of stomatal conductance and vapor pressure
167	difference from leaf intercellular spaces to bulk atmosphere. The hydro-dynamic module
168	represents a plant's roots, xylem, and foliage as a variably porous media (Sperry, Adler,
169	Campbell, & Comstock, 1998) with conductance and capacitance changing in response to tissue
170	water potentials dictated by the pressure-volume (P-V) curve and the pressure-conductance
171	(vulnerability) curve (Manzoni et al. 2013, Christoffersen et al. 2016). Stomatal conductance is
172	modified from the Ball-Berry model (Ball et al. 1984, Oleson et al. 2013, Fisher et al. 2015) with
173	a further constraint of leaf water potential through a water stress index βt , defined by a function
174	of the ratio of the leaf water potential to the leaf water potential of half stomatal closure (P50gs)
175	(Christoffersen et al. 2016). The soil column is divided into a given number of 20 layers. The

proportion of roots in each layer is calculated from Zeng's (2001) two parameter power law

177 function. Water flow from each soil layer within the root zone into the plant root system is

calculated as a function of the hydraulic conductance determined by root biomass and root traits

- such as specific root length, and the difference in water potential between the absorbing roots
- and the rhizosphere, and -the transpiration is the sum of root water uptake from all soil layers.
- Additional technical details and parameter sensitivity analysis can be found in the technical notes
- 182 (FATES Development Team, 2021, https://fates-users-guide.readthedocs.io/projects/tech-
- doc/en/latest/index.html) and publications (e.g. Koven et al., 2020; Xu et al., 2023, Ding et al.,
- 184 2023a, 2023b, Robbins et al, 2024).
- The version of FATES-Hydro used in this study also includes representation of the
- mechanisms by which soil hypoxia and salinity impact tree physiology and mortality (Ding
- 187 2023b). The complete description of these new developments can be found in Ding et al.
- 188 (2023b). Below we describe the root loss function because this is the key component in this
- 189 study.
- The root loss function (kr_{red}), expressed as the proportion of the root conductance under
- normal condition, is composed of hypoxia reduction ($kr_{red,sat}$) and the salinity reduction ($kr_{red,sat}$),
- 192 expressed as:

$$kr_{red} = kr_{red,sat} \cdot kr_{red,sal}$$
 Eq.1

- Each term varies between near zero to 1, with near zero means no roots and 1 means the roots grow as normal.
- The <u>hypoxia saturation</u> reduction ratio is given as:

$$kr_{red,sat} = \frac{1}{1 + b \cdot e^{ks(x - x_0)}}$$
 Eq.2

- where *b* and *ks* are the scaling parameters that determine the rate of fine root loss from saturation; *x* (hours) is the total duration of the volumetric soil water content [m3/m3] exceeds
- 200 90% saturation over a defined previous period of x_0 . Biologically, parameter b and ks can be used
- 201 to represent how well the root system of the trees are adapted to waterlogging condition (Fig S2).
- The salinity reduction ratio is given by a salinity cumulation term (acc_sal) as:

203 $kr_{red,sal} = exp(-kc*acc_{sal})$ Eq.3a $acc_{sal} = max[0, \sum (Sal_{soil,t} - Sal_{cr})]$ 204 Eq.3b 205 where kc is a parameter determining the rate of fine root loss due to salinity, and $\pm acc_{sal}$ 206 represents the cumulative salinity stress, calculated by summing the difference between soil 207 $\underline{\text{salinity}}$ ($Sal_{soil,t}$) and a critical threshold (Sal_{cr}) beyond which salinity starts to negatively affect 208 root mass, over all timesteps (i) up to the current step n. All terms are in PSU. As this 209 formulation is dependent on the model's timestep, all simulations were run with a fixed temporal 210 resolution of 30 minutes. where kc is a parameter determining the rate of fine root loss due to salinity; acc_{sal} (PSU) is the cumulative salinity since simulation starts, $Sal_{soil,t}$ is the soil salinity 211 at a given time, Sal_{cr} is the critical soil salinity beyond which salinity starts to negatively affect 212 213 root mass. 214 215 2.2.2 Parameterization and benchmarking 216 For the pine and the salinity induced root loss rate, the parameters used in Ding et al. (2023) 217 were used in this study. For the broadleaf trees at Lake Erie, the parameters used in FATES-218 Hydro were either from field observations or obtained from the TRY trait database (Kattge et al., 219 2011) when field observation were not available (Table S1). V_{cmax} was estimated from A/Ci

were used in this study. For the broadleaf trees at Lake Erie, the parameters used in FATES-Hydro were either from field observations or obtained from the TRY trait database (Kattge et al., 2011) when field observation were not available (Table S1). V_{cmax} was estimated from A/Ci curves and then adjusted within the observed range so that the simulated hourly A_{net} matched the fitted line of observed values (Fig. S2). P50_{gs} was adjusted within the ranges of the temperate broadleaf trees from the TRY database so that the simulated hourly leaf water potential matches the fitting curved based on measured hourly LWP (Fig. S2).

The allometry parameters that define the relationships between diameter at breast height and total tree height, sapwood area, total woody biomass, and total leaf biomass were estimated based on values of the Biomass and Allometry Database (BAAD) (Falster et al., 2015). The complete list of parameters can be found in the GitHub repository:

228 https://github.com/JunyanDing/FATES_COMPASS.

220

221

222

223

224

225

226

To calibrate the plant hydraulic parameters, K_{max} and xylem vulnerability curves, we first adjusted the parameters within the observed range of values for our broadleaf species (Kattge et al. 2011) from TRY database of the site to be close to measured hourly values and then we adjusted the phenology parameters so that the decline of simulated sap flow matched the observed pattern (FigS4 top panel). For saturation induced root loss function, based on previous studies (Islam and Macdonald 2004, Aroca et al. 2012, Karlova et al. 2021) and unpublished experimental observations (B. Wolf unpublished data), we set x_0 to 120 hours (5 days) for this study. We then adjusted the root loss parameter ks so simulated sap flow was close to the mean of the observed values (FigS4 bottom panel) at the shoreline location with observed water table depth. The simulated average daily sap flow at upland and shoreline locations matches well with observations (Fig. 2). While perfect agreement is not expected, we find that the model reasonably captures the seasonal pattern and interannual variability of sap flow.

229

230

231

232

233

234

235

236

237

238

239

240

241

242

243

244

245

246

247

248

249

250

251

252

253

254

255

256

257

258

259

For the marsh grass, we use the biochemical and physiological parameters from O'Meara et al. (2021) and the allometry (height and total leaf area to stem width ratio) was estimated based on GCReW data (https://serc.si.edu/gcrew/data). Because marsh plants are annual or bi-annual, phenology and maximum density (number of individuals per ground area), which control the variation of total leaf area, play a more important role in marsh ecosystems than plant physiology Because marsh plants are annual or bi-annual, phenology and maximum density (number of individuals per ground area) that control the variation of total leaf play more important role in marsh ecosystems than plant physiology. We specifically calibrated these parameters. The phenology parameters are estimated based on the NDVI values from Yaping et al. (2022) and the 2022 field measurement of sap flow at the LE upland site. The phenology parameters are same for both marsh plants and broadleaf trees, meaning marsh plant and broadleaf trees have same leaf on and off times. The NDVI values at the neighboring wetlands indicate the marsh grass system had an LAI ~2 (m² m⁻²) during the peak growing season. We further constrained the maximum density of the marsh to a growing season LAI of 2 m² m⁻². To calibrate the broadleaf trees, we ran the model at LE site in 2022 initialized by the inventory data, then compared the model output with the field observations of photosynthesis, leaf water potential (Fig S2), and sap flow (Fig S3). We confirmed that the simulated growth rates over the 30-year simulation period fell within the observed range of tree ring widths measured from tree cores (Fig \$4\$5). Note, our goal was to assess if simulated growth rates were within the range of observations to enable hypothesis tests, not to reproduce observed interannual growth variability at the individual tree level.

2.2.3 Setup of numerical experiments

The numerical experiments involved three plant functional types (PFT): broadleaf deciduous tree, evergreen conifer tree, and herbaceous marsh plants. We will call them broadleaf tree, conifer tree, and marsh plants hereafter. Each simulation was constructed either as broadleaf tree-marsh or as conifer tree-marsh combination. We first simulated the LE site using its native vegetation, the broadleaf trees and marsh, and the CB site using its native vegetation, conifer trees, and marsh. We then swapped the tree types between sites, such that the broadleaf forest was simulated at CB and the conifer forest at LE. The simulations of virtual forests at each site allowed investigation of how different forest types may respond to the differing drivers, i.e., with and without salinity. For both experiments we also examined the ecosystem-scale consequences of forest loss, namely on total evapotranspiration and photosynthetic carbon fluxes.

The simulations were driven by the University of East Anglia Climatic Research Unit (CRU) Japanese Reanalysis (JRA) meteorological product (CRUJRA) (University of East Anglia Climatic Research Unit; Harris, 2019) for 1990 through 2019. The simulations were initialized with inventory data of upland locations for the trees at both sites (Fig. S1). We used the observed inventory data of *Carya spp.* at LE for both CB and LE initialization and observed inventory data of *Pinus spp.* at CB for both CB and LE initialization. The simulated marsh colonization was from external seed supply at the first year, then from both external seed supply and local reproduction afterward.

Daily soil salinity and water table depth at CB and water table depth at LE were used as external driving factors. We used empirically estimated soil salinity at CB, by regression based on open water level and salinity (Ding et al. 2023b). To estimate water table depth at LE from 1990 to 2019, we obtained the water level of LE at the station in Cleveland (https://tidesandcurrents.noaa.gov/inventory.html?id=9063063). We fit a linear correlation between the station water level and the observed water table depth at the LE shoreline location in 2022 (Fig 1a), then used this linear model to estimate the daily water depth from 1990 to 2019 via the station water data (Fig 1a). During the simulation period, two floods occurred at LE

(1997–1999 and 2016–2019); at CB, salinity slightly rose around 2002 and 2009, followed by a constant increase after 2012 (Fig 1d and 1e).

Root loss was driven by soil hypoxia (indexed by the duration of saturated water content) for LE, and both soil hypoxia and salinity for CB. At LE, the root loss was calculated based on water table depth. The parameters that govern root loss were calibrated based on measured sap flow, leaf water potential, and loss of plant hydraulic conductance (S1). At CB, the additive root loss was estimated from soil salinity because soil salinity is highly coupled with hypoxia at CB, and we used the parameter values from Ding et al. (2023b). Root loss was simulated similarly for both species to explicitly examine the extent to which differences in phenology, leaf and stem physiology, and the lack of species-specific information on hypoxia and salinity tolerance may result in different mortality patterns.

3. Results of numerical experiment

3.1 Inundation impacts on tree physiology and mortality

Inundation had similar impacts on the broadleaf and conifer trees at both LE and CB. Root loss increased over time as water levels rose (Fig 2a3a, b). However, root loss differed between sites, particularly after 2015, due to the differences in inundation dynamics. At LE, root loss increased each year as water levels rose, but root growth during periods of low water levels allowed partial recovery. In contrast, the chronic increase in inundation and soil salinity at CB after 2015 led to ongoing root loss because there was less seasonal variation in water level (Fig. 1c and d), and hence no opportunity for recovering root biomass. This difference in root loss between sites resulted in sustained reductions in hydraulic conductance (k/k_{max}) at CB after 2015, whereas both species at LE exhibited some recovery each year (Fig. 3c, d).

Despite these site level differences, both LE and CB experienced severe declines in k/k_{max} by the end of the simulation period. Non-structural carbohydrates (NSC) showed only slight variation over the simulation period, suggesting that loss of hydraulic conductance was the primary process underlying mortality (Fig. 3e, f). This is consist with observed %NSC at Lake Erie site (Ttable \$2\$3). Mortality of both the broadleaf and conifer trees increased after 2015, with higher mortality at CB than LE (Fig. 3g, h). Increasing root loss was associated with

318 declining k/k_{max} (Fig. 4a, b) and increased whole-tree mortality (Fig. 4c, d), with no difference 319 between species. The declines in k/k_{max} were strongly associated with increased mortality (Fig. 320 4). 321 3.2 Ecosystem consequences of forest loss 322 3.2.1 Broadleaf simulations at Lake Erie and Chesapeake Bay 323 We examined the ecosystem-scale consequences of mortality on leaf area index (LAI), gross 324 primary production (GPP), transpiration (E_t), and root water uptake with the broadleaf 325 simulations at both the LE and CB shoreline sites. In these simulations, the loss of leaf area 326 through inundation-driven tree mortality was compensated by marsh invasion, resulting in stable 327 ecosystem-scale LAI over time (Fig. 5a, 5b). GPP and E_t showed somewhat similar patterns as 328 LAI for both sites, again due to marsh invasion as trees died (Fig. 5c-f). GPP was slightly higher 329 in the shoreline than the upland sites due to the higher GPP of marsh plants, and Et showed slight 330 declines below the upland sites (Fig. 5b and 5c). While LAI, GPP, and E_t all showed relative 331 stability over time, the loss of trees and the marsh invasion led to large changes in the depths of 332 water uptake at both LE and CB. The change in vegetation dominance associated with tree 333 mortality led to an increase in shallow water uptake and a decline in deep water uptake (Fig. 5g-334 j). 335 3.2.2 Conifer simulations at Lake Erie and Chesapeake Bay 336 The conifer simulations at the shoreline sites at both LE and CB exhibited different patterns 337 than the broadleaf species. LAI, GPP, and E_t all declined with tree loss, which was not 338 compensated for due to limited marsh invasion (Fig. 6a-f). There was no change in shallow water 339 uptake with changes in vegetation dominance, but there was a large decline in deep water uptake 340 (Fig. 6g-j). As tree LAI declined with mortality, the increase in shallow water uptake observed 341 for broadleaf species was not observed for the conifer species, whereas both species exhibited 342 declines in deep water uptake (Fig. $\frac{76}{}$). 343 4. Discussion 344 4.1 Summary of Major Findings 345 We conducted numerical experiments at two coastal sites to investigate the mechanisms

driving inundation-driven tree mortality and the subsequent ecosystem impacts and how they

differ across tree species and with different inundation regimes. The simulations indicated that root loss was the dominant step driving mortality via hydraulic failure for both species and at both sites (Fig. 3 and 4). Replacement of broadleaf trees by marsh resulted in increased LAI and GPP but reduced E_T at both sites (Fig 5a to 5f). Replacement of conifer trees by marsh result in reduced LAI, GPP, and E_T at both sites (Fig. 6a to 6f). Transition from forests to marsh shifted root water uptake from deep to shallow soil layers (Fig 4g, 4h, 6g, 6h). Our numerical experiments suggest that the same mechanisms caused forest loss at both sites regardless of tree type, whereas the ecosystem effects from the replacement of forest by marsh differed between broadleaf and conifer forests. Future empirical studies should be conducted to verify these findings.

4.2 Tree Level Effects

Root loss can promote tree mortality through hydraulic failure and carbon starvation (McDowell et al., 2022). Our simulations indicated that hydraulic failure is the dominant process underlying tree mortality for broadleaf and conifer trees at both sites (Fig. 3 and 4). Root loss resulted in decreased whole tree hydraulic conductance and subsequently xylem conductivity due to increased xylem embolism (Fig. 4a and 4b). Overall, this led to an increase in tree mortality (Fig. 4c and 4d). These effects were consistent between LE and CB, although they exhibited different temporal patterns due to variation in the inundation regimes. Moreover, similar effects of root loss on plant hydraulics have been documented in both modeling studies (Li et al., 2022; Ding et al., 2023b) and field studies (Zaerr, 1983; Pezeshki et al., 1996; Andersen et al., 1984; Islam and Macdonald, 2004; Aroca et al., 2012; Karlova et al., 2021).

Reduced hydraulic conductivity can lower leaf water potential and causes stomatal closure. This mechanism can result in reduced photosynthesis and negative carbon balance, resulting in reduced capability to maintain tissues and defend against insects and pathogens (McDowell et lal., 2022). However, simulated non-structural carbohydrates (NSC) values (Fig. 3e and 3f) suggest that carbon starvation was not a major process of tree mortality at the shoreline locations of both study sites and for both tree types. These results were unexpected. We had anticipated that broadleaf trees might experience greater carbon limitation due to higher leaf area and photosynthetic demand. However, the simulations demonstrated that hydraulic failure associated with root loss occurred before significant depletion of NSC, leading to similar mortality

trajectories between the two species. This may be due to the rate of inundation-driven root loss relative to the rate of NSC decline (Ding et al., 2023b). The LE and CB inundation regimes had periods when inundation declined and the salinity at CB was relatively low, allowing a low level of ongoing photosynthesis to replenish their NSC pools. Carbon starvation is a slow process due to the time required to draw down NSCs, whereas hydraulic failure can occur rapidly (McDowell et al., 2022).

Simulated k/k_{max} and mortality of broadleaf and conifer trees changed similarly with root loss (Fig. 4), despite large differences between the two species in their leaf economic traits, wood anatomy, crown allometry, and phenology. This similarity arose because whole-tree k/k_{max} can only be as high as the lowest k/k_{max} of any pathway between the soil and foliage. Whole-tree hydraulic conductance is constrained by the lowest conductance along the soil–plant–atmosphere pathway. In our simulations, root loss strongly reduced soil-to-root conductance, which therefore set the limit for whole-tree k/k_{max}. Root loss caused the soil-to-root k/k_{max} to decline dramatically, forcing whole tree k/k_{max} to equal soil-to-root k/k_{max}. Thus, traits and processes downstream from the roots became less important due to the dominant role of root loss in promoting hydraulic failure when it becomes severe (Fig. 3c, d, g, h). Both species are poorly adapted to high levels of hypoxia or salinity, thus root loss was the critical failure point in tree survival under inundation. Species with root systems adapted to inundation, such as mangroves, may experience different consequences of increased flooding that could lead to a larger role of carbon starvation such as through ion toxicity to photosynthesis and leaf loss (Munns and Termaat, 1986).

This convergence in response does not imply that all species react identically to inundation. Rather, it reflects that under the modeled conditions, root system failure overwhelms the contributions of other physiological differences. While these results offer mechanistic insights, the lack of empirical data on species-specific root adaptations remains a limitation. We note that our parameterizations were based on representative species (Carya, Quercus, and Pinus), which we treated as proxies for the two tree types. Outcomes may differ among other species within these groups, therefore As such, we caution against overgeneralization and recommend interpreting these results as hypothesis-generating rather than conclusive. Future research on the cross-species variation of root loss and downstream mortality mechanisms, and explicitly test

whether these findings extend to the broader PFT level, will be useful to advance transferable predictive capacity of coastal vegetation change under increasing inundation.

409

407

408

410

411

412

413

414

415

416

417

418

419

420

421

422

423

424

425

426

427

428

429

430

431

432

433

434

435

436

4.3 Ecosystem-Level Effects Between the Forest Types and Sites

The ecosystem-scale consequences of coastal forest loss result both from the loss of trees and the invasion of marsh plants. We found differences in the ecosystem consequences associated with species but not sites. As tree mortality associated with soil inundation and/or salinity progressed, marsh plants invaded broadleaf systems more rapidly than coniferous systems, thus resulting in different impacts on GPP and Et. Marsh plants invaded when LAI declined below 1 m²/m² in both systems (Fig. 5a, 5b and 6a, 6b). The conifer system had higher stand density than the broadleaf system resulting in initial LAI values of $\sim 4 \text{ m}^2/\text{m}^2$ and $\sim 2 \text{ m}^2/\text{m}^2$, respectively, thus a much larger amount of mortality was required in the conifer system for LAI to decline by 1 m²/m²; in other words, when canopy opened hereby facilitated marsh invasion and establishment. The mortality rates were similar for both species (Fig. 3); thus, the differences in marsh invasion were due primarily to initial stand structure rather than to species composition or mortality rates per se. The declining LAI in the CB with increasing mortality is consistent with remotely sensed estimates of the normalized difference vegetation index (Chen and Kirwan 2022), and the rates of marsh invasion are consistent with other observations (Kirwan and Gedan, 2019; McKown and Burdick, 2024). This resulted in increasing GPP in the broadleaf system because marsh plants have higher photosynthetic capacity than trees (Pan et al., 2020) and because ecosystem LAI was higher after marsh invasion into the broadleaf system (Fig. 5c, 5d and 6c, 6d). In contrast, the slower invasion of marsh plants into the conifer system caused ecosystem level GPP to decline with tree mortality.

Replacing broadleaf forest by marsh increased GPP slightly, while E_t declined slightly (Fig. 7c and 7d). This is likely due to the higher water-use efficiency of marsh plants than trees. E_t declined with tree mortality in both systems, but more so in the conifer system (Figs 5e, 5f and 6e, 6f). These changes were associated with increased water uptake from shallow soil layer and reduced uptake from the deep soil layer due to the shallower roots of the marsh plants (Fig. 8) (Maitre et al., 1999; Schenk and Jackson, 2002). In contrast, conifer mortality resulted in less

marsh invasion and hence reductions in GPP and E_t (Fig. 7), and water uptake from both shallow and deep soil layers was greatly reduced due to the loss in conifer roots that were not compensated by marsh plants (Fig. 8).

440

441

442

443

444

445

446

447

448

449

450

451

452

453

454

455

456

457

458

459

460

461

462

463

464

465

466

437

438

439

4.5 Future Research

Our numeric experiments revealed critical mechanisms regulating vegetation dynamics and ecosystem impacts in response to SLR. Our study also revealed key next steps to improve our understanding and model representation. We found that root loss drives large declines in k/k_{max} that result in increasing mortality and marsh invasion. However, we did not directly measure root distribution, but instead calibrated parameters using observed data on leaf water potential, sap flow, and the k/k_{max}. We then applied these calibrated parameters with the assumption that both the broadleaf and conifer had similar root responses to hypoxia and salinity. This decision was based on three factors. First, we had no species-specific data on root conductance and mortality in response to hypoxia and salinity. Second, both species live at the shoreline margins of their respective regions, and thus, we assume they are similar in their root responses. Third, the rooting depths at both sites are shallow, thus rooting depth may not vary significantly across species. By setting the root loss parameters the same for both tree species, we investigated whether differences in phenology, leaf and stem physiology traits result in different mortality patterns between the two species and found that these trait differences have negligible impacts. Given the critical role of root conductance and survival, field studies to explore root structure and function are important next steps for coastal systems. Ecosystem manipulation experiments can be particularly powerful to untangle the impact of hypoxia and salinity on root loss and subsequent impacts on physiology and survival, enabling cause-and-effect tests that enable improved predictive understanding of tree mortality in coastal systems (e.g., Hopple et al., 2023).

The role of changing stand structure during ghost forest formation may be an important factor impacting marsh invasion, the physiology of surviving trees, and the recruitment of new trees. Changes in light availability as mortality increases aided marsh invasion and promoted higher photosynthesis and recruitment (Fig 5a and 5b, Fig 6a and 6b) (Kirwan and Gedan, 2019). The reduction of water uptake from deep layers may promote hypoxia, salinity, and changes in redox potential and nutrient cycling. With forest cover, high deep-water uptake can enhance

infiltration of rainfall into deep soil layers, which can bring oxygen rich surface water and nutrients to these deep layers. Reduced infiltration could result in lower dissolved oxygen in deep soil (Foulquier et al., 2010), increased salinity (Kirwan et al. in review), changed redox potential (Rubol et al., 2012), and decreased nutrient availability (Burgin et al., 2010; Burgin et al., 2012) all of which should feedback to limit vegetation growth. Therefore, quantifying the rate of marsh invasion, survival of remaining trees, and recruitment of tree seedlings is necessary to identify mechanisms associated with changing light availability and belowground processes.

In addition, it is important to interpret our results in the context of projected future climate change and sea-level rise. Chesapeake Bay is expected to continue experiencing sea-level rise of approximately 3–6 mm yr⁻¹, about twice the global average, while the Great Lakes are projected to undergo increasingly variable water levels under climate change (Kayastha et al., 2022; Sallenger et al., 2012; Ezer and Corlett, 2012). These projections imply that inundation events will become more frequent and prolonged, thereby intensifying the mechanisms identified in our study, particularly root loss leading to hydraulic failure. Rising temperatures and elevated CO₂ may further modify these dynamics by altering tree water demand, photosynthetic rates, and marsh productivity, though the net effects remain uncertain. Together, these changes suggest heightened vulnerability of both broadleaf and conifer coastal forests to conversion into marshes, with ecosystem-scale consequences for carbon cycling and hydrology. These broader climate—hydrology interactions are examined in more detail in a separate manuscript (Ding et al., *in review* at JGR–Biogeosciences), where we provide more detailed projections.

4.6 Summary

Our numerical experiments indicated that root loss due to coastal inundation served as the driving force behind the transition from forest to marsh through hydraulic failure-induced tree mortality. This mechanism resulted in similar physiological consequences for both broadleaf and conifer trees. However, the transition from forests to marshes led to different ecosystem impacts between broadleaf and conifer forests due to their different initial LAI. Future research aimed at enhancing our understanding and representation of the interplay among physiological, demographic, and stand structural processes in different forest types is necessary for better predicting vegetation dynamics and ecosystem consequences under SLR.

496	Acknowledgments
497	JD, NM, BBL, KM, NW, JPM, PR, SCP, MW, TM, PT, and VB were supported by the
498	Department of Energy, Biological and Environmental Research program project Coastal
499	Observations, Mechanisms, and Predictions Across Scales (COMPASS). Any use of trade,
500	product or firm names is for descriptive purposes only and does not imply endorsement by the
501	U.S. Government. MK acknowledges the support of the U.S. National Science Foundation
502	(#1654374, #1832221, #2012670).
503	Author contributions
504	JD and NM designed the study and drafted the manuscript. JD developed the model and
505	performed simulations. CDK helped with model development. NM, NW, LS, DD, KM, MK, PR
506	PZ, HZ, SP, SW, WW, WI, AS, TM, and PT collected field data and performed data analysis.
507	All the authors contributed to the manuscript.
508	Competing interests
509	None declared
510	Code availability statements
511	The data and FATES-Hydro code that support the findings of this study are openly
512	available in GitHub repository: https://github.com/JunyanDing/FATES_COMPASS or zendo:
513	https://doi.org/10.5281/zenodo.15116449

- 515 References
- Aroca, R., Porcel, R., and Ruiz-Lozano, J. M.: Regulation of root water uptake under abiotic
- stress conditions, J. Exp. Bot., 63, 43–57, https://doi.org/10.1093/jxb/err266, 2012.
- Acosta-Motos, J. R., Ortuño, M. F., Bernal-Vicente, A., Diaz-Vivancos, P., Sanchez-Blanco, M.
- J., and Hernandez, J. A.: Plant responses to salt stress: Adaptive mechanisms, Agronomy, 7, 18,
- 520 2017.
- Arkema, K. K., Guannel, G., Verutes, G., Wood, S. A., Guerry, A., Ruckelshaus, M., Kareiva,
- P., Lacayo, M., and Silver, J. M.: Coastal habitats shield people and property from sea-level rise
- 523 and storms, Nat. Clim. Change, 3, 913–918, , 2013.
- Barbier, E. B.: Valuing ecosystem services for coastal wetland protection and restoration:
- Progress and challenges, Resources, 2, 213–230, , 2013.
- Barbier, E. B., Hacker, S. D., Kennedy, C., Koch, E. W., Stier, A. C., and Silliman, B. R.: The
- value of estuarine and coastal ecosystem services, Ecol. Monogr., 81, 169–193, 2011.
- Ball, M. C., Farquhar, G. D., and Box, P. O.: Photosynthetic and stomatal responses of two
- 529 mangrove species, Aegiceras corniculatum and Avicennia marina, to long-term salinity and
- 530 humidity conditions, Plant Physiol., 74,
- 531 https://academic.oup.com/plphys/article/74/1/1/6079345, 1984.
- Burlakova, L. E., Karatayev, A. Y., Pennuto, C., and Mayer, C.: Changes in Lake Erie benthos
- over the last 50 years: Historical perspectives, current status, and main drivers, J. Great Lakes
- 534 Res., 40, 560–573, 2014.
- Clites, A. H., Smith, J. P., Hunter, T. S., and Gronewold, A. D.: Visualizing relationships
- between hydrology, climate, and water level fluctuations on Earth's largest system of lakes, J.
- 537 Great Lakes Res., 40, 807–811, , 2014.
- Dasgupta, S. and Meisner, C.: Climate change and sea level rise: A review of the scientific
- 539 evidence, , , 2009.
- Davidson, I. C., Cott, G. M., Devaney, J. L., and Simkanin, C.: Differential effects of biological
- invasions on coastal blue carbon: A global review and meta-analysis, Glob. Change Biol., 24,
- 542 5218–5230, 2018.
- 543 Ding, J., Buotte, P., Bales, R., Christoffersen, B., Fisher, R. A., Goulden, M., Knox, R.,
- Kueppers, L., Shuman, J., Xu, C., and Koven, C. D.: Understanding the interplay of rooting and
- 545 hydraulic strategies on the response of conifer forest stands to multiyear drought in the Southern
- Sierra Nevada of California, Biogeosciences, 20, 4491–4510, https://doi.org/10.5194/bg-20-
- 547 4491-2023, 2023.
- 548 Ding, J., McDowell, N., Fang, Y., Ward, N., Kirwan, M. L., Regier, P., Megonigal, P., Zhang,
- P., Zhang, H., Wang, W., and Li, W.: Modeling the mechanisms of conifer mortality under
- seawater exposure, New Phytol., https://doi.org/10.1111/nph.19076, 2023.
- Ding, J., Nate McDowell, Nate Conroy, Donnie J. Day, Yilin Fang, Kenneth M. Kemner,
- Matthew L. Kirwan, Matthew Kovach, Patrick Megonigal, Kendalynn A. Morris, Teri O'Meara,
- 553 Stephanie C. Pennington, Roberta B. Peixoto, Peter Thornton, Mike Weintraub, Peter Regier,

- Leticia Sandoval, Fausto Machado-Silva, Alice Stearns, Nicholas D. Ward, Stephanie J. Wilson,
- Vanessa Bailey: Investigating coastal vegetation dynamics and ecosystem impacts under
- elevated CO₂ and temperature: a mechanistic modeling approach, *in review*, JGR-Biogeoscience
- Duarte, C. M., Losada, I. J., Hendriks, I. E., Mazarrasa, I., and Marbà, N.: The role of coastal
- plant communities for climate change mitigation and adaptation, Nat. Clim. Change, 3, 961–968,
- 559 2013.
- Du, Y., Zhang, Y., and Shi, J.: Relationship between sea surface salinity and ocean circulation
- and climate change, Sci. China Earth Sci., 62, 771–782, 2019.
- Ezer, T. and Corlett, W. B.: Analysis of relative sea-level variations and trends in the
- Chesapeake Bay: Is there evidence for acceleration in sea level rise?, in: Proc. MTS/IEEE
- Oceans 2012, Hampton Roads, USA, 14–19 October 2012,
- 565 <u>https://doi.org/10.1109/OCEANS.2012.6404930</u>
- Fisher, R. A., Muszala, S., Verteinstein, M., Lawrence, P., Xu, C., McDowell, N. G., Knox, R.
- G., Koven, C., Holm, J., Rogers, B. M., and Spessa, A.: Taking off the training wheels: The
- properties of a dynamic vegetation model without climate envelopes, CLM4.5(ED), Geosci.
- 569 Model Dev., 8, 3593–3619, 2015.
- 570 Fisher, R. A., Koven, C. D., Anderegg, W. R. L., Christoffersen, B. O., Dietze, M. C., Farrior, C.
- 571 E., Holm, J. A., Hurtt, G. C., Knox, R. G., Lawrence, P. J., et al.: Vegetation demographics in
- 572 Earth System Models: A review of progress and priorities, Glob. Change Biol., 24, 35–54,
- 573 https://doi.org/10.1111/gcb.13910, 2018.
- 574 Friedman, A. R., Reverdin, G., Khodri, M., and Gastineau, G.: A new record of Atlantic sea
- 575 surface salinity from 1896 to 2013 reveals the signatures of climate variability and long-term
- 576 trends, Geophys. Res. Lett., 44, 1866–1876, 2017.
- 577 Frieswyk, C. B. and Zedler, J. B.: Vegetation change in Great Lakes coastal wetlands: Deviation
- from the historical cycle, J. Great Lakes Res., 33, 366–380, 2007.
- Gedan, K. B., Kirwan, M. L., Wolanski, E., Barbier, E. B., and Silliman, B. R.: The present and
- future role of coastal wetland vegetation in protecting shorelines: Answering recent challenges to
- the paradigm, Clim. Change, 106, 7–29, 2011.
- Hopple, A. M., Doro, K. O., Bailey, V. L., et al.: Attaining freshwater and estuarine-water soil
- saturation in an ecosystem-scale coastal flooding experiment, Environ. Monit. Assess., 195, 425,
- 584 https://doi.org/10.1007/s10661-022-10807-0, 2023.
- Hosoda, S., Suga, T., Shikama, N., and Mizuno, K.: Global surface layer salinity change detected
- by Argo and its implication for hydrological cycle intensification, J. Oceanogr., 65, 579–586,
- 587 2009.
- Hudon, C.: Impact of water level fluctuations on St. Lawrence River aquatic vegetation, Can. J.
- 589 Fish. Aquat. Sci., 54, 2853–2865, 1997.
- Islam, M. A. and Macdonald, S. E.: Ecophysiological adaptations of black spruce (Picea
- mariana) and tamarack (Larix laricina) seedlings to flooding, Trees, 18, 35–42, 2004.

- McKown, J. G. and Burdick, D. M.: Salt marsh migration into coastal uplands and application
- for conservation in New Hampshire, Great Bay National Estuarine Research Reserve, 45 pp.,
- https://scholars.unh.edu/jel/681/, 2024.
- Karlova, R., Boer, D., Hayes, S., and Testerink, C.: Root plasticity under abiotic stress, Plant
- 596 Physiol., 187, 1057–1070, 2021.
- Kayastha, M. B., Ye, X., Huang, C., and Xue, P.: Future rise of the Great Lakes water levels
- 598 under climate change, J. Hydrol., 612, 128205, 2022.
- 599 Keddy, P. A. and Reznicek, A. A.: Great Lakes vegetation dynamics: The role of fluctuating
- water levels and buried seeds, J. Great Lakes Res., 12, 25–36, 1986.
- Koven, C. D., Knox, R. G., Fisher, R. A., Chambers, J. Q., Christoffersen, B. O., Davies, S. J.,
- Detto, M., Dietze, M. C., Faybishenko, B., Holm, J., Huang, M., Kovenock, M., Kueppers, L.
- M., Lemieux, G., Massoud, E., and Xu, C.: Benchmarking and parameter sensitivity of
- 604 physiological and vegetation dynamics using the Functionally Assembled Terrestrial Ecosystem
- Simulator (FATES) at Barro Colorado Island, Panama, Biogeosciences, 17, 3017–3044,
- 606 https://doi.org/10.5194/bg-17-3017-2020, 2020.
- Kirwan, M. L. and Gedan, K. B.: Sea-level driven land conversion and the formation of ghost
- 608 forests, Nat. Clim. Change, 9, 450–457,, 2019.
- Kirwan, M. L. and Megonigal, J. P.: Tidal wetland stability in the face of human impacts and
- 610 sea-level rise, Nature, 504, 53–60, 2013.
- Larcher, W.: Physiological plant ecology: ecophysiology and stress physiology of functional
- groups, Springer, Berlin, 2003.
- 613 Le Maitre, D. C., Scott, D. F., and Colvin, C.: Review of information on interactions between
- vegetation and groundwater, 1999.
- 615 Lindsey, R.: Climate change: Global sea level, Climate.gov, https://www.climate.gov/news-
- 616 features/understanding-climate/climate-change-global-sea-level, accessed 14 August 2020, 2021.
- 617 Lukac, M., Pensa, M., and Schiller, G.: Tree species' tolerance to water stress, salinity, and fire,
- in: Forest Management and the Water Cycle: An Ecosystem-Based Approach, pp. 247–261,
- 619 Springer, Dordrecht, 2011.
- Manzoni, S.: Integrating plant hydraulics and gas exchange along the drought-response trait
- 621 spectrum, Tree Physiol., 34, 1031–1034, https://doi.org/10.1093/treephys/tpu088, 2014.
- McDowell, N. G., Ball, M., Bond-Lamberty, B., Kirwan, M. L., Krauss, K. W., Megonigal, J. P.,
- Mencuccini, M., Ward, N. D., Weintraub, M. N., and Bailey, V.: Processes and mechanisms of
- 624 coastal woody-plant mortality, Glob. Change Biol., 28, 5881–5900,
- 625 https://doi.org/10.1111/gcb.16297, 2022.
- Mimura, N.: Sea-level rise caused by climate change and its implications for society, Proc. Jpn.
- 627 Acad. Ser. B, 89, 281–301, 2013.
- Mitsch, W. J., Bernal, B., and Hernandez, M. E.: Ecosystem services of wetlands, Int. J.
- 629 Biodivers. Sci. Ecosyst. Serv. Manag., 11, 1–4, 2015.

- Niknam, S. R. and McComb, J.: Salt tolerance screening of selected Australian woody species –
- 631 a review, For. Ecol. Manage., 139, 1–19, 2000.
- Munns, R. and Termaat, A.: Whole-plant responses to salinity, Funct. Plant Biol., 13, 143–160,
- 633 1986.
- 634 O'Meara, T. A., Thornton, P. E., Ricciuto, D. M., Noyce, G. L., Rich, R. L., and Megonigal, J.
- P.: Considering coasts: Adapting terrestrial models to characterize coastal wetland ecosystems,
- 636 Ecol. Model., 450, 109561, 2021.
- Oleson, K. W., Lawrence, D. M., Bonan, G. B., Drewniak, B., Huang, M., Koven, C. D., and
- Yang, Z.: Technical description of version 4.5 of the Community Land Model (CLM), NCAR
- Technical Note, https://opensky.ucar.edu/islandora/object/technotes:515, 2013.
- Pan, Y., Cieraad, E., Armstrong, J., Armstrong, W., Clarkson, B. R., Colmer, T. D., Pedersen,
- O., Visser, E. J. W., Voesenek, L. A. C. J., and van Bodegom, P. M.: Global patterns of the leaf
- economics spectrum in wetlands, Nat. Commun., 11, 4519, https://doi.org/10.1038/s41467-020-
- 643 18354-3, 2020.
- Robbins, Z., Chambers, J., Chitra-Tarak, R., Christoffersen, B., Dickman, L. T., Fisher, R.,
- Jonko, A., Knox, R., Koven, C., Kueppers, L., and McDowell, N.: Future climate doubles the
- risk of hydraulic failure in a wet tropical forest, New Phytol., 244, 2239–2250, 2024.
- Saber, A., Cheng, V. Y., and Arhonditsis, G. B.: Evidence for increasing influence of
- atmospheric teleconnections on water levels in the Great Lakes, J. Hydrol., 616, 128655, 2023.
- Sallenger, A. H., Doran, K. S., and Howd, P. A.: Hotspot of accelerated sea-level rise on the
- Atlantic coast of North America, Nat. Clim. Change, 2, 884–888,
- https://doi.org/10.1038/nclimate1597, 2012
- 652 Sairam, R. K., Kumutha, D., Ezhilmathi, K., Deshmukh, P. S., and Srivastava, G. C.: Physiology
- and biochemistry of waterlogging tolerance in plants, Biol. Plant., 52, 401–412, 2008.
- 654 Schenk, H. J. and Jackson, R. B.: The global biogeography of roots, Ecol. Monogr., 72, 311–328,
- 655 2002.
- Shin, S., Gronewold, A. D., Fry, L. M., Hong, Y., Cannon, D., and Fujisaki-Manome, A.: Long-
- term hydroclimate trends in the Great Lakes basin: Are there hotspots of regional change?, J.
- 658 Hydrol. Reg. Stud., 59, 102347, https://doi.org/10.1016/j.ejrh.2025.102347, 2025
- Shepard, C. C., Crain, C. M., and Beck, M. W.: The protective role of coastal marshes: A
- systematic review and meta-analysis, PLoS One, 6, e27374, 2011.
- 661 Silliman, B. R., He, Q., Angelini, C., Smith, C. S., Kirwan, M. L., Daleo, P., Renzi, J. J., Butler,
- J., Osborne, T. Z., Nifong, J. C., and van de Koppel, J.: Field experiments and meta-analysis
- reveal wetland vegetation as a crucial element in the coastal protection paradigm, Curr. Biol., 29,
- 664 1800–1806, , 2019.
- Sippo, J., Lovelock, C. E., Santos, I. R., Sanders, C. J., and Maher, D. T.: Mangrove mortality in
- a changing climate: An overview, Estuar. Coast. Shelf Sci., 215, 241–249,
- 667 https://doi.org/10.1016/j.ecss.2018.10.011, 2018.

- 668 Smith, I. M., Fiorino, G. E., Grabas, G. P., and Wilcox, D. A.: Wetland vegetation response to
- record-high Lake Ontario water levels, J. Great Lakes Res., 47, 160–167, 2021.
- 670 Spalding, M. D., Ruffo, S., Lacambra, C., Meliane, I., Hale, L. Z., Shepard, C. C., and Beck, M.
- W.: The role of ecosystems in coastal protection: Adapting to climate change and coastal
- 672 hazards, Ocean Coast. Manag., 90, 50–57, 2014.
- 673 Sperry, J. S., Adler, F. R., Campbell, G. S., and Comstock, J. P.: Limitation of plant water use by
- 674 rhizosphere and xylem conductances: Results from a model, Plant Cell Environ., 21, 347–357,
- 675 https://doi.org/10.1046/j.1365-3040.1998.00287.x, 1998.
- Taherkhani, M., Vitousek, S., Barnard, P. L., Frazer, N., Anderson, T. R., and Fletcher, C. H.:
- Sea-level rise exponentially increases coastal flood frequency, Sci. Rep., 10, 1–17, , 2020.
- Theuerkauf, E. J., Braun, K. N., Nelson, D. M., Kaplan, M., Vivirito, S., and Williams, J. D.:
- 679 Coastal geomorphic response to seasonal water-level rise in the Laurentian Great Lakes: An
- example from Illinois Beach State Park, USA, J. Great Lakes Res., 45, 1055–1068, 2019.
- Thiéblemont, R., Le Cozannet, G., D'anna, M., Idier, D., Belmadani, A., Slangen, A. B., and
- Longueville, F.: Chronic flooding events due to sea-level rise in French Guiana, Sci. Rep., 13,
- 683 21695, 2023.
- Theuerkauf, E. J. and Braun, K. N.: Rapid water level rise drives unprecedented coastal habitat
- loss along the Great Lakes of North America, J. Great Lakes Res., 47, 945–954, 2021.
- 686 Ury, E. A., Yang, X., Wright, J. P., and Bernhardt, E. S.: Rapid deforestation of a coastal
- landscape driven by sea-level rise and extreme events, Ecol. Appl., 31, e02339, 2021.
- Varekamp, J. C., Thomas, E., and Van de Plassche, O.: Relative sea-level rise and climate
- change over the last 1500 years, Terra Nova, 4, 293–304, 1992.
- Vineis, P., Chan, Q., and Khan, A.: Climate change impacts on water salinity and health, J.
- 691 Epidemiol. Glob. Health, 1, 5–10, 2011.
- Wilcox, D. A.: Implications of hydrologic variability on the succession of plants in Great Lakes
- 693 wetlands, Aquat. Ecosyst. Health Manag., 7, 223–231, 2004.
- Wilcox, D. A. and Nichols, S. J.: The effects of water-level fluctuations on vegetation in a Lake
- 695 Huron wetland, Wetlands, 28, 487–501, 2008.
- Zeng, X.: Global vegetation root distribution for land modeling, J. Hydrometeorol., 2, 525–530,
- 697 2001.
- Zhao, C., Zhang, H., Song, C., Zhu, J. K., and Shabala, S.: Mechanisms of plant responses and
- adaptation to soil salinity, The Innovation, 1, 100017, 2020.
- Zhang, P., McDowell, N. G., Zhou, X., Wang, W., Leff, R. T., Pivovaroff, A. L., Zhang, H.,
- 701 Chow, P. S., Ward, N. D., Indivero, J., and Yabusaki, S. B.: Declining carbohydrate content of
- Sitka-spruce trees dying from seawater exposure, Plant Physiol., 185, 1682–1696,
- 703 https://doi.org/10.1093/plphys/kiab002, 2021.

Zhou, J., Zhang, J., Chen, Y., Qin, G., Cui, B., Lu, Z., Wu, J., Huang, X., Thapa, P., Li, H., and Wang, F.: Blue carbon gain by plant invasion in saltmarsh overcompensated carbon loss by land reclamation, Carbon Res., 2, 39, 2023.

Figure caption

- Fig.1 Study area: a) relation between lake depth and soil water table depth in 2022, at the Lake
- 710 Erie site transition zone corresponding to the shoreline location in simulations; b) depth of Lake
- 711 Erie 1990–2020; c) Estimated water table depth at Lake Erie (LE) shoreline location; d) sea level
- and open water salinity of the nearby station of Chesapeake Bay (CPB); and e) Estimated soil
- 713 salinity at CPB site

714

708

Fig.2 Benchmark root loss function by comparing measured and simulated average daily sap flow of Aug and Sep. 2022 at upland location and shoreline location at LE site

717

Fig.3 Simulated tree level variables of shoreline forest at Lake Erie and Chesapeake Bay: a) and b) monthly mean % live root; c) and d) monthly mean k/k_{max}; e) and f) annual %NSC; g) and h) annual mortality rate

721

Fig.4 Simulated relation between a) and b) mean growing season k/k_{max} and % live roots of tree; c) and d) annual mean mortality and % live roots of tree

724 725

726

727

Fig.5 Ecosystem effects of broadleaf forest at Lake Erie and Chesapeake Bay: a) and b) mean growing season leaf area index (LAI); c) and d) gross primary productivity (GPP); e) and f) transpiration (E_t); g) and h) root water uptake rate from shallow soil; i) and j) root water uptake rate from deep soil at shoreline (SH) and upland (UP) locations

728729730

731

732

Fig.6 Ecosystem effects of conifer forest at Lake Erie and Chesapeake Bay: a) and b) mean growing season leaf area index (LAI); c) and d) gross primary productivity (GPP); e) and f) transpiration (E_t); g) and h) root water uptake rate from shallow soil; i) and j) root water uptake rate from deep soil at shoreline (SH) and upland (UP) locations

733734

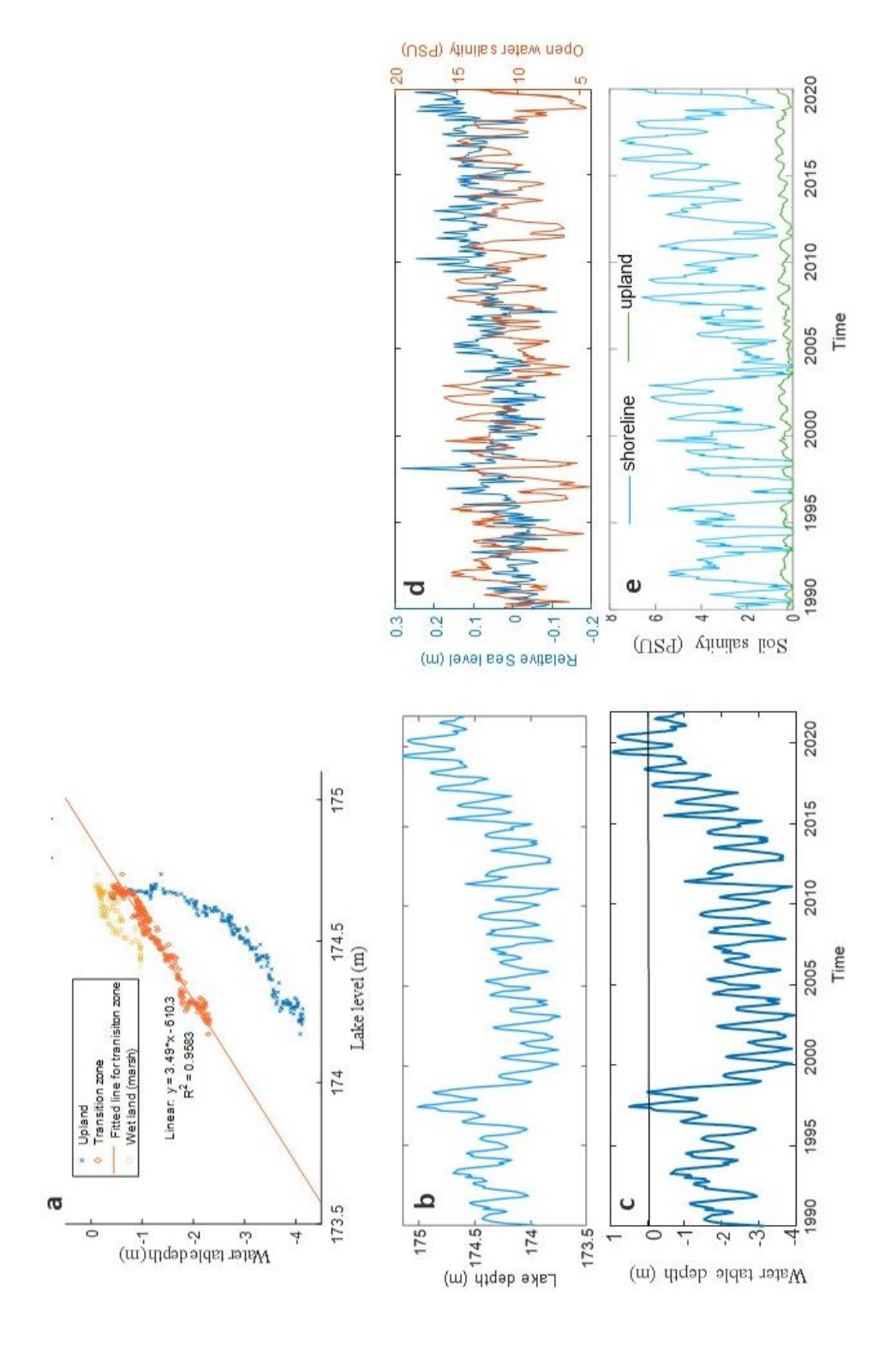
Fig. 7 Change in gross primary productivity (GPP) (a and b) and transpiration (E_t) (c and d) with tree abundance of shoreline forests as indicated by tree LAI at Lake Erie and Chesapeake Bay

737

Fig.8 Change in water uptake from shallow soil layer (a and b) and from deep soil layer (c and d) with tree abundance of shoreline forests as indicated by tree LAI at Lake Erie and Chesapeake
Bay

Figures

Fig.1



Page 26 of 33

Fig. 2

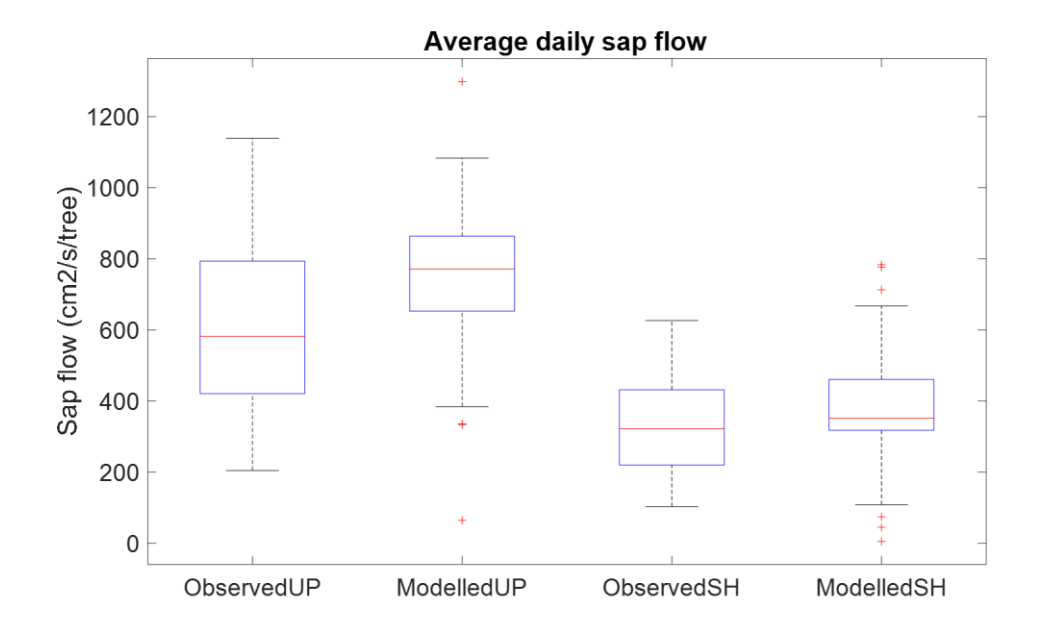


Fig.3

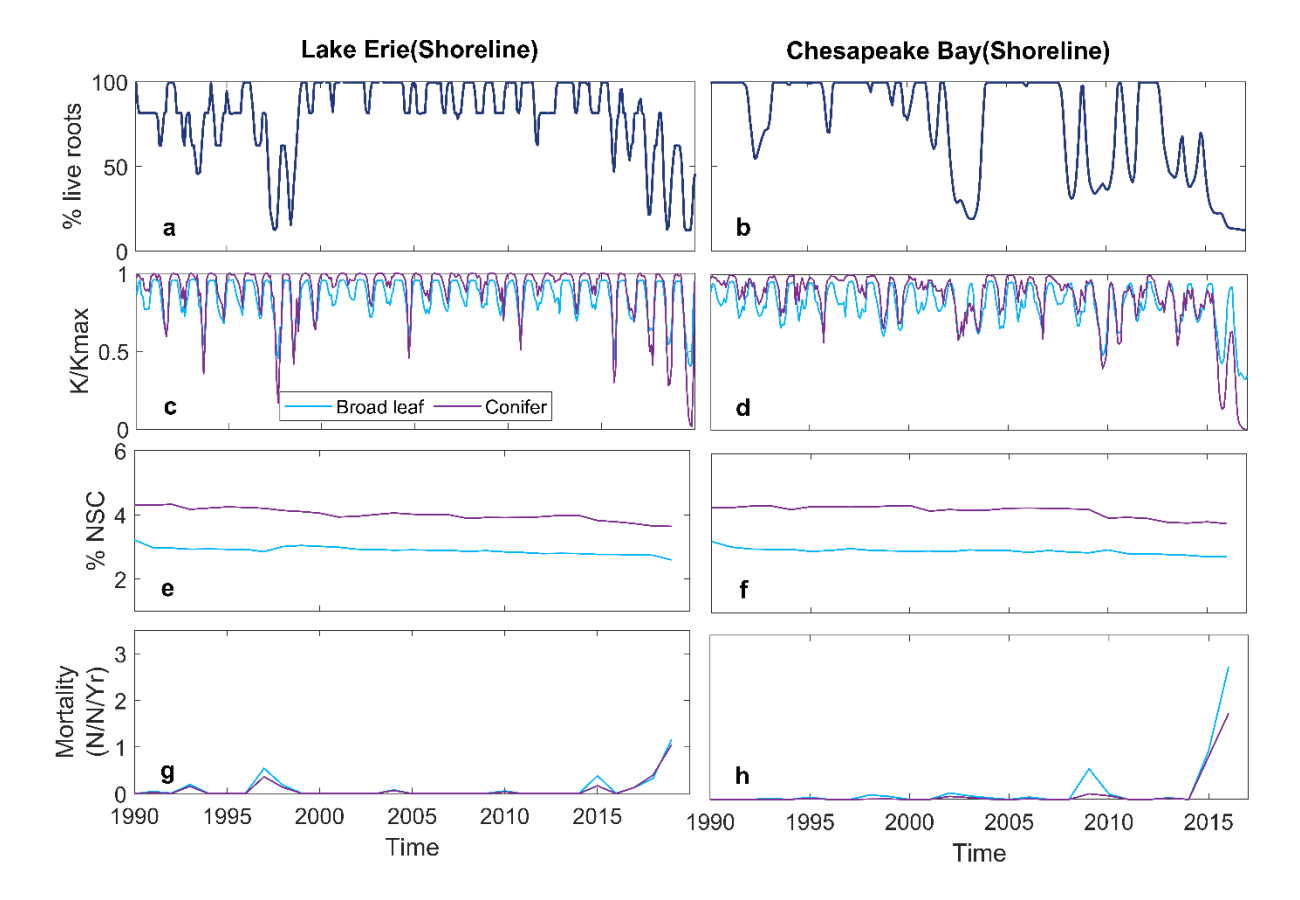


Fig.4

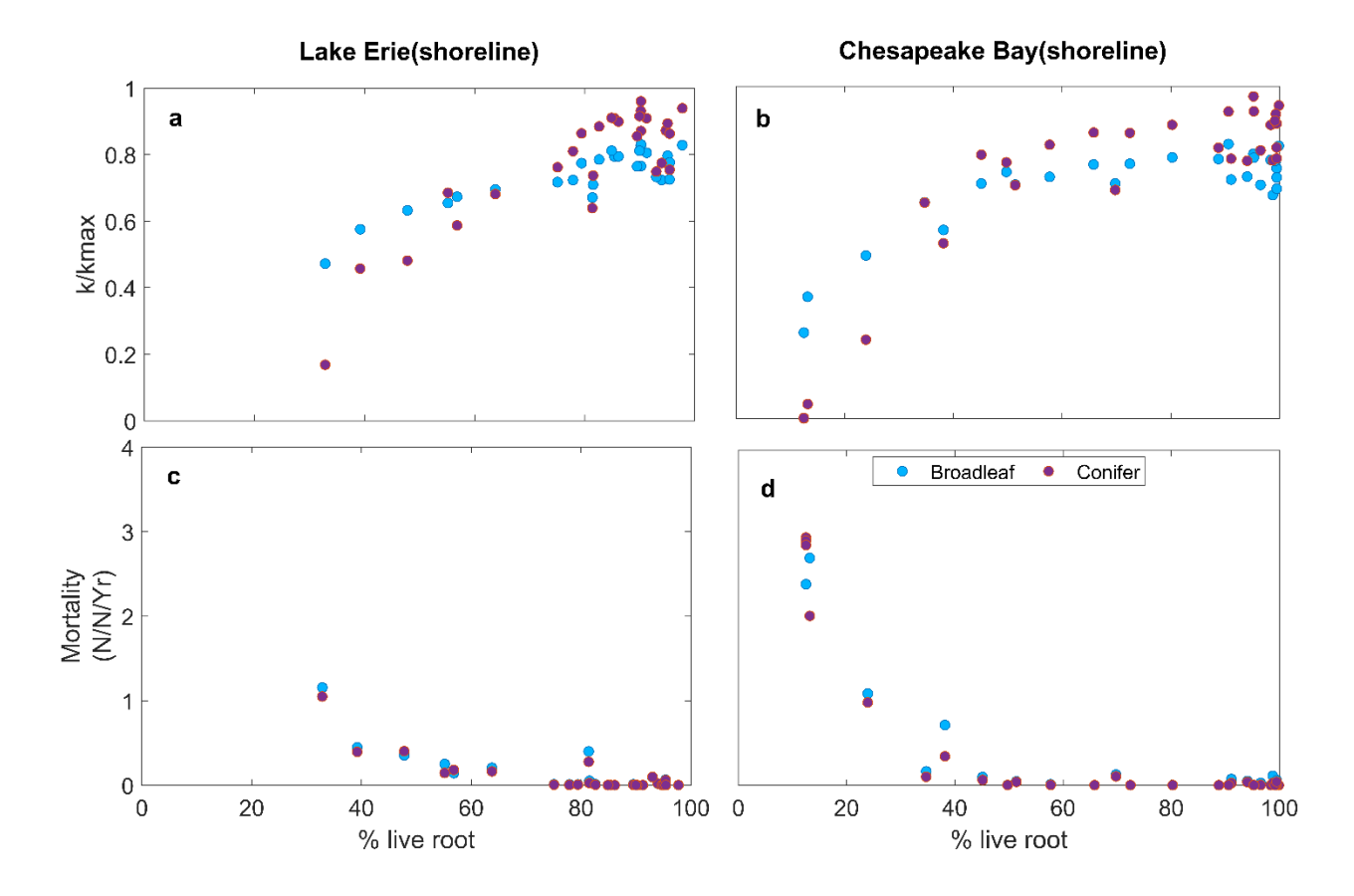


Fig.5



Fig.6

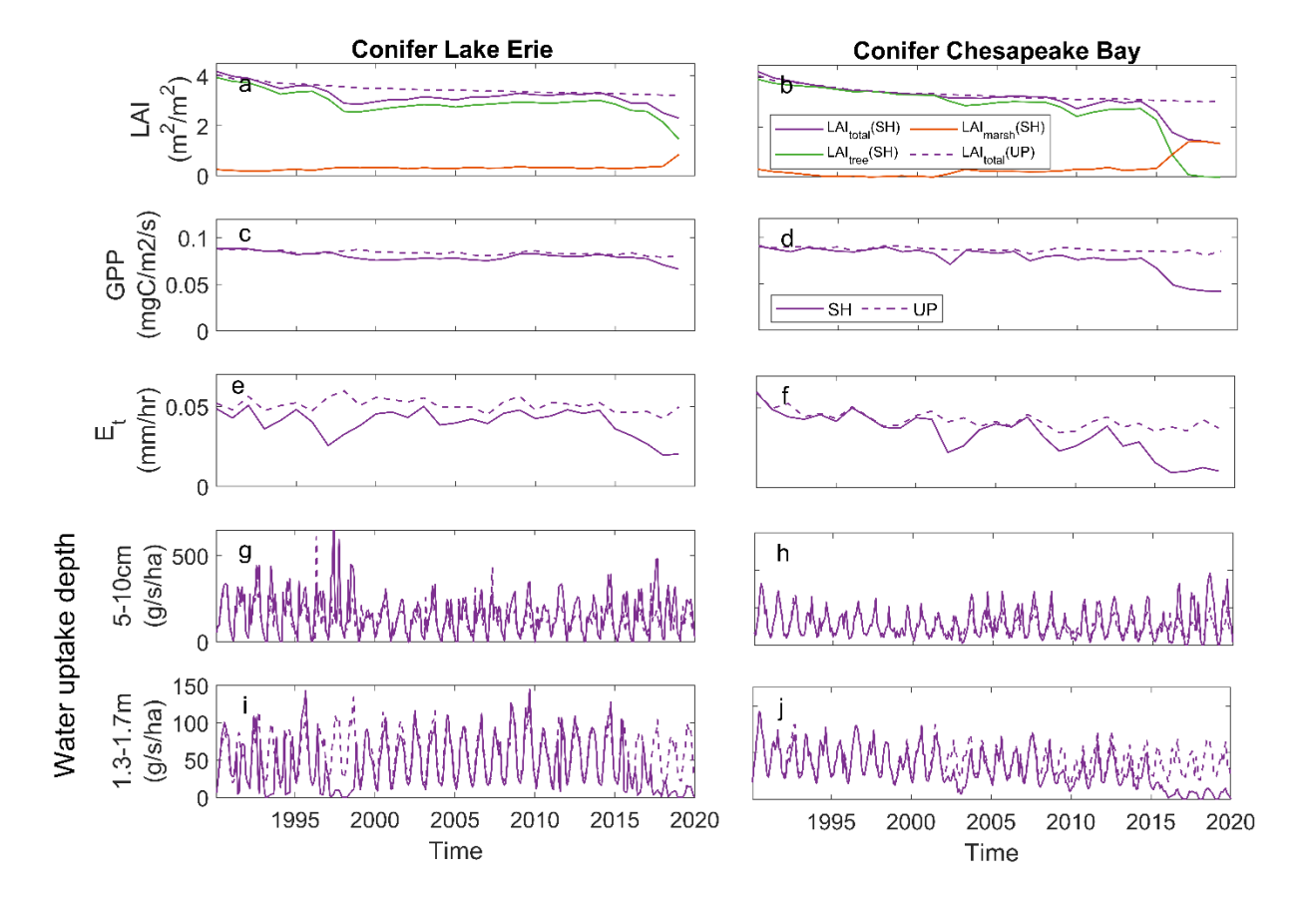


Fig. 7

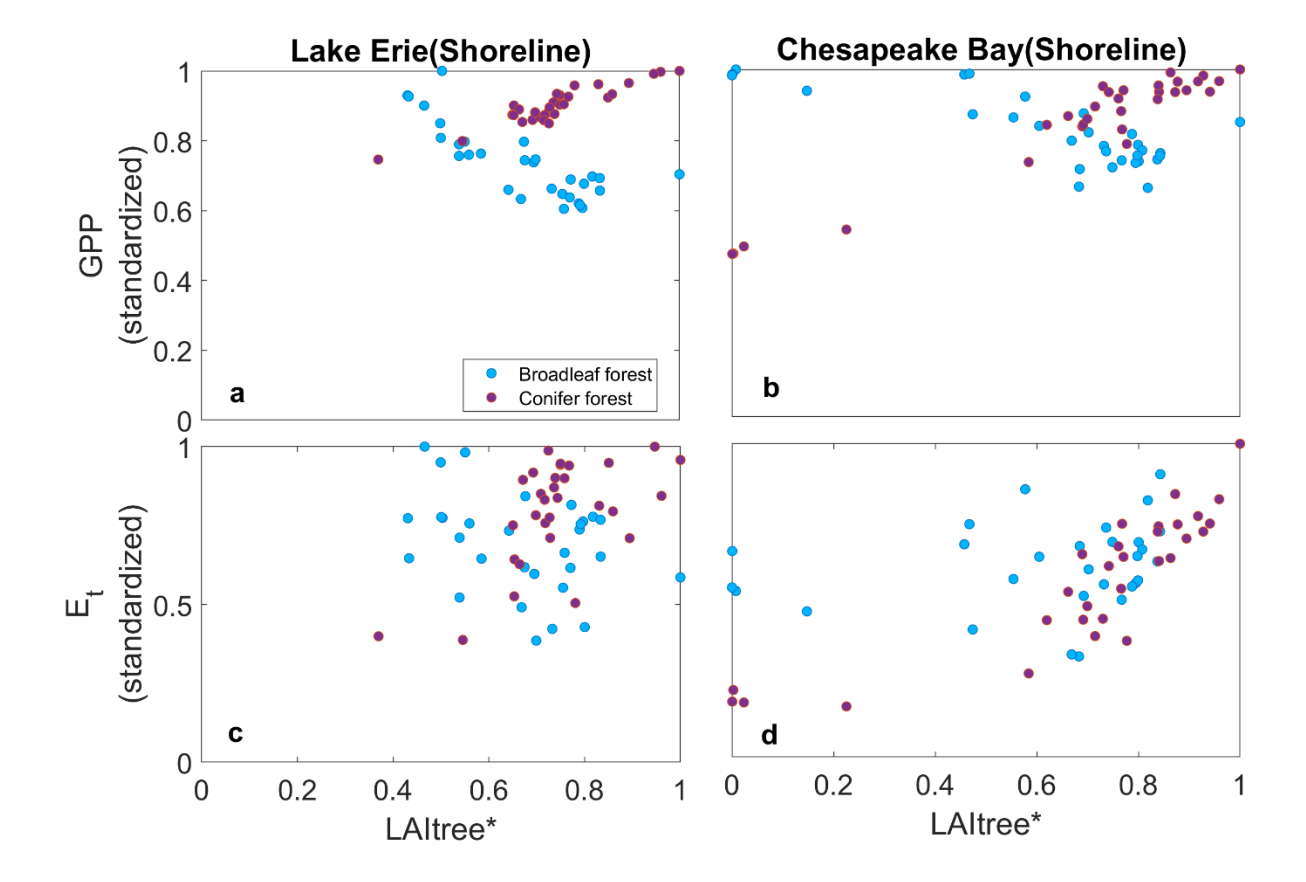


Fig.8

